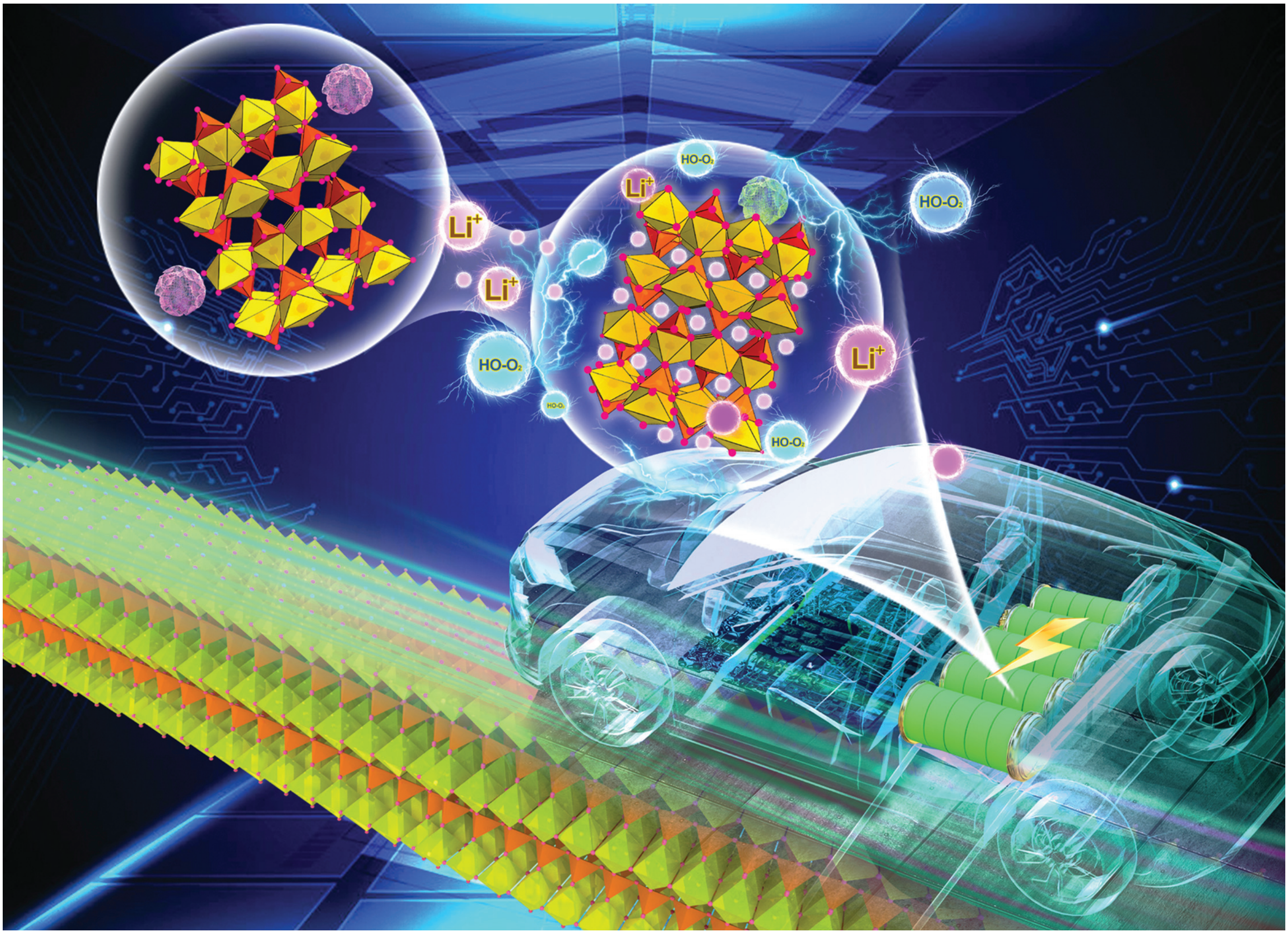

Showcasing research by Professor Dan Tsang *et al.* from The Hong Kong Polytechnic University, Hong Kong, China.

Low-carbon recycling of spent lithium iron phosphate batteries *via* a hydro-oxygen repair route

This approach involved disassembly of retired batteries, followed by separation of cathode electrode and selective extraction of lithium by hydro-oxygen species. The extracted lithium was used in crystal reconstruction to restore the batteries as new ones that can be reused in electric vehicles. This approach can promote low-carbon and environmentally friendly recycling of retired lithium iron phosphate batteries globally, contributing to sustainable future and reducing carbon emissions.

As featured in:

See Dan Tsang *et al.*, *Green Chem.*, 2023, **25**, 6642.

ROYAL SOCIETY OF CHEMISTRY

rsc.li/greenchem

Green Chemistry

ROYAL SOCIETY OF CHEMISTRY

PAPER

View Article Online
View Journal | View Issue

Cite this: *Green Chem.*, 2023, **25**, 6642

Low-carbon recycling of spent lithium iron phosphate batteries *via* a hydro-oxygen repair route†

Kang Liu,[a,e] Junxiong Wang,[b] Mengmeng Wang,[a,e] Qiaozhi Zhang,[a] Yang Cao,[a] Longbin Huang,[c] Marjorie Valix[d] and Daniel C. W. Tsang *[a,e]

Received 10th February 2023,
Accepted 9th June 2023

DOI: 10.1039/d3gc00472d

rsc.li/greenchem

In this study, we proposed a sequential and scalable hydro-oxygen repair (HOR) route consisting of key steps involving cathode electrode separation, oxidative extraction of lithium (Li), and lithium iron phosphate ($LiFePO_4$) crystal restoration, to achieve closed-loop recycling of spent $LiFePO_4$ batteries. A hydro-oxygen environment (with a cathode electrode : H_2O_2 ratio of 30 g mL^{-1}) was first used to achieve non-destructive separation of the $LiFePO_4$ cathode material and aluminum foil within a short period of time (0.25 min). The selective and high-efficiency extraction of Li from exfoliated $LiFePO_4$ cathode materials was subsequently achieved by mechanochemically coupled oxidation potential regulation (conditions: 10 min, a rotational speed of 1000 rpm, and a $LiFePO_4$ cathode material : H_2O_2 ratio of 1 : 37.5 g mL^{-1}). The $LiFePO_4$ crystals were successfully restored *via* a solid phase sintering process using the extracted Li and residual iron phosphate framework, and the regenerated $LiFePO_4$ crystal exhibited a considerable specific electrochemical capacity (~151.2 mA h g^{-1}, 1C), which is comparable to that of commercial cathode materials. A life cycle assessment demonstrated that the HOR route can significantly reduce carbon emissions by −0.38 kg CO_2 eq. and smog release by −0.17 kg O_3 eq. per kg of spent $LiFePO_4$ batteries, thus contributing to a circular economy and global decarbonization.

1. Introduction

The electrification of mass transportation is widely accepted by communities and industries as an effective solution for global decarbonization.[1–4] In 2021, global sales of electric vehicles surpassed 2 million.[5,6] Lithium-ion batteries (LIBs) are the core component of electric vehicles, determining their driving performance.[7,8] Lithium iron phosphate ($LiFePO_4$; LFP) batteries have been the preferred choice for electric vehicle assembly among commercialized Li-ion batteries due to their lower costs, better thermal and chemical stability, and longer life cycle.[9–12] In 2021, the global energy supply from LFP batteries reached 172.1 GW h, indicating a year-on-year growth rate of 219.6%.[5] The recent growth in the global supply of LFP batteries faces challenges due to price fluctuations and an unstable supply of critical metals, particularly cobalt (Co), which is used for ternary Li-ion batteries.[13–15] The capacity of LFP batteries fades with age, and they have a limited lifespan, typically lasting between 6 and 8 years.[16–19] Cascade utilization will continue to decrease the power capacity of LFP batteries, ultimately leading to their dismantling and recycling/disposal.[5,20–22] Due to enormous growth in the use of LIBs, a significant amount of spent LFP batteries will become a secondary source of Li if they can be efficiently recycled and recovered.[23] This is an important research area that deserves extensive attention in the coming years.[12,24,25]

Hydrometallurgy is a widely recognized strategy for extracting lithium (Li) from LFP cathode materials, but it faces critical challenges such as economic sustainability due to the loss of Li and thin profit margins.[26–32] The Li-free iron phosphate ($FePO_4$) residue is a low-value solid waste that contributes to economic costs and environmental burdens due to its disposal issues.[33–37] Considering the high production cost of LFP crystals and the weakened economic drivers of recovery, developing a cost-effective and environmentally friendly approach to

---

[a] *Department of Civil and Environmental Engineering, The Hong Kong Polytechnic University, Hung Hom, Kowloon, Hong Kong, China. E-mail: dan.tsang@polyu.edu.hk*
[b] *Frontiers Science Center for Transformative Molecules, School of Chemistry and Chemical Engineering, Shanghai Jiao Tong University, Shanghai 200240, China*
[c] *Ecological Engineering of Mine Wastes, Sustainable Minerals Institute, The University of Queensland, Brisbane, Qld 4072, Australia*
[d] *School of Chemical and Biomolecular Engineering, University of Sydney, New South Wales 2006, Australia*
[e] *State Key Laboratory of Clean Energy Utilization, Zhejiang University, Hangzhou 310027, China*

† Electronic supplementary information (ESI) available. See DOI: **https://doi.org/10.1039/d3gc00472d**

recover and restore the crystal structure of spent cathode materials is a crucial driver for the sustainable recycling of LFP batteries.[38–40]

Studies have shown that the capacity decay of LIBs can mainly be attributed to the gradual depletion of Li in LFP cathode materials.[41–43] This decay occurs because Li, referred to as 'dead Li', cannot be relocated due to changes in the chemical environment within the battery, ultimately resulting in the deactivation of the crystals.[44,45] Pre-lithiation and high-temperature annealing are the main approaches used for repairing spent LFP cathode materials.[46,47] Pre-lithiation involves Li doping of the anode to mitigate the irreversible capacity loss of the electrode.[25,47] Chen *et al.*[48] reported an efficient battery regeneration technology, referred to as defect-directed repair, which regenerates spent LFP batteries through aqueous solution pre-lithiation at 180 °C for 5 h followed by rapid annealing at 400–800 °C. This defect-specific regeneration technique was found to significantly reduce energy consumption by 80–90% and greenhouse gas emissions by approximately 75% when compared to hydrometallurgical and pyrometallurgical routes. Jing *et al.*[49] proposed repairing the active crystal compounds in spent LFP batteries through a hydrothermal reduction approach. In this process, Li was replenished under hydrothermal conditions of 200 °C for 3 h with 12 g L^{-1} of Li_2SO_4, an L/S ratio of 6 mL g^{-1}, and 1.0 mL of hydrazine hydrate. The repaired LFP crystals demonstrated excellent charge and discharge properties at 0.2C (with a capacity of 146.2 mA h g^{-1}) in a new electrochemical cycle.

Compared with Li extraction by pyrometallurgical or hydrometallurgical processes, regeneration appears to be an economical and promising technological strategy for recycling spent LFP batteries.[34,39,41,50–53] Nonetheless, critical challenges remain in the regeneration process to repair spent LFP batteries.[54] For instance, a pollution-free strategy for separating the cathode material from the aluminum (Al) foil in spent LFP batteries still needs to be developed to minimize lithium loss.[55,56] The application of pyrometallurgy to recycle spent LFP batteries unavoidably incurs environmental concerns, including the release of organic fluorine,[57] organic solvents from using *N*-methylpyrrolidone,[58–60] and dust from mechanical crushing of the cathode electrode.[61,62] The regeneration route is dominated by high-temperature solid-state Li replenishment and/or hydrothermal reduction, which consume large amounts of exogenous and corrosive chemicals.[63,64] The existing pre-lithiation routes for LFP crystals typically require high temperatures (180–240 °C) and long reaction times (3–12 h), resulting in an extended regeneration cycle, high energy consumption, and poor economic advantages.[65] Among different electrode materials, LFP is considered to produce the most greenhouse gases (GHGs) when compared to lithium nickel cobalt manganese oxides ($LiNi_xCo_yMn_zO_2$; $x + y + z = 1$), lithium cobaltate ($LiCoO_2$), and lithium manganese oxide ($LiMnO_2$).[16] The high carbon emissions resulting from the current processing of LFP crystal repair negate the original purpose of large-scale application of LFP batteries, which should serve to achieve sustainable development goals.[66] As a result, there is an urgent need to establish novel, pollution-free, short-range, and low-carbon routes for recycling and regenerating spent LFP batteries.[67]

This study proposes a hydro-oxygen repair (HOR) route based on the crystal characteristics of LFP to enable low-carbon battery regeneration. The spent LFP battery cathode materials can be successfully regenerated using hydrogen peroxide (H_2O_2) through an integrated process that consists of the following key steps: non-destructive separation of the cathode electrode, hydro-oxygen oxidative extraction of residual Li, and restoration of LFP crystals. Effective separation avoids the loss of Li, damage to the Al foil, and dust pollution while hydro-oxygen extraction of Li avoids the use of corrosive chemicals. The proposed HOR route can significantly reduce carbon and pollutant emissions with the potential to make an essential contribution to global carbon neutrality.

2. Materials and methods

2.1. Materials and reagents

Spent LFP batteries were purchased from the network agent of Build Your Dreams (BYD Co., Ltd), Shenzhen, China. The chemicals used in this study, including hydrogen peroxide (H_2O_2, mass fraction of 30% v/v), glucose ($C_6H_{12}O_6$, AR, ≥98.0%), hydrochloric acid (HCl, CP, 36.0–38.0%), and nitric acid (HNO_3, CP, 65.0–68.0%), were purchased from Sigma-Aldrich.

2.2. Experimental procedures

Our proposed HOR route for repairing spent LFP batteries is shown in Fig. 1. Spent LFP batteries were first subjected to a discharge experiment using a self-designed lighting device. After manual cutting and disassembling, the plastic case, cathode electrode, anode electrode, and separator were obtained (Table S1†). The graphite and copper foil of the anode electrode were separated by sonication in deionized water. The obtained cathode electrode was used for HOR experiments.

In particular, the HOR route can be divided into three stages:

(I) Hydro-oxygen separation of the cathode electrode: first, the spent LFP cathode electrode was cut to a regular shape of 1.0 cm × 5.0 cm coupons. The hydro-oxygen reaction medium for the separation stage was composed of 50 mL of deionized water with varying volumes of H_2O_2 solution (1.0, 2.0, 3.0, 4.0, and 5.0 mL). The cathode electrode coupons were added and exposed to the hydro-oxygen reaction medium for pre-determined times (0.25, 0.5, 1.0, 2.0, 3.0, 4.0, and 5.0 min; room temperature and atmospheric pressure without stirring). During the hydro-oxygen reaction, the generated oxygen bubbles separated the LFP cathode material from the Al foil. The separated LFP cathode material (named S-LFP) and Al foil were taken out for the next step. The resulting hydro-oxygen solution medium was filtered through a 0.45 μm membrane and then digested with 5 mL of HNO_3 for elemental analysis

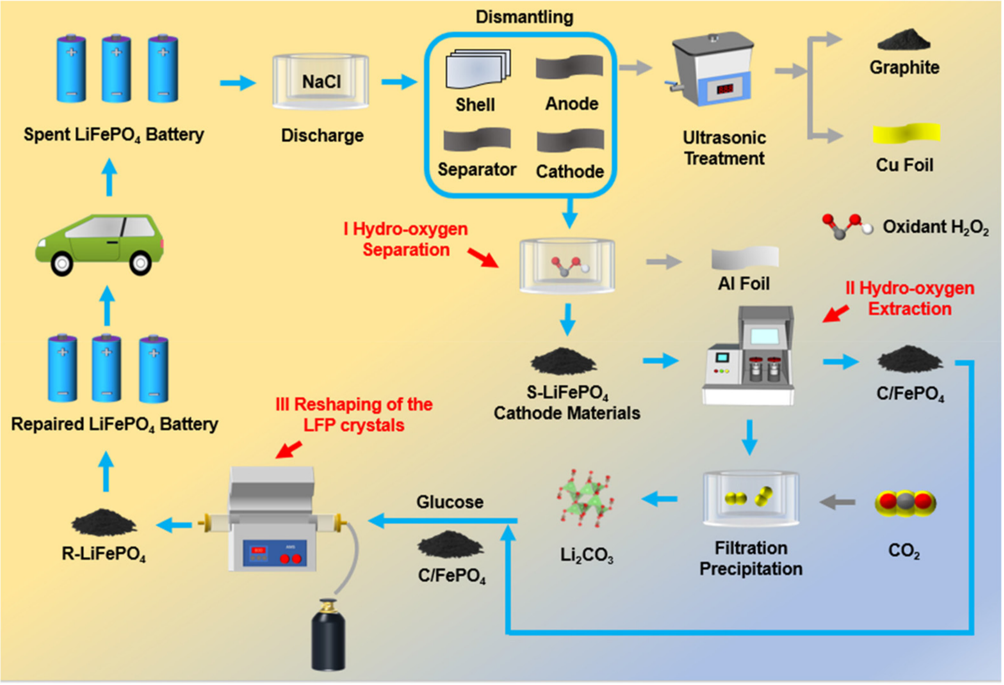

Fig. 1 Proposed HOR route for repairing spent LFP batteries.

by inductively coupled plasma optical emission spectroscopy (ICP–OES, Agilent 5110, U.S.A.).

(II) Hydro-oxygen extraction of Li: approximately 0.2 g of spent LFP piece was weighed precisely and added to H_2O_2 with a solid/liquid ratio (g mL^{-1}) of 1 : 12.5, 1 : 25, 1 : 37.5, and 1 : 50. The mixture was transferred to a polytetrafluoroethylene pot in a high-energy mechanochemical reaction device (DECO-PBM-AD-0.4 L, Deco Technology Development Co., Ltd, Changsha, China). The mechanochemical extraction experiments were carried out at rotational speeds of 0, 200, 400, 600, 800, and 1000 rpm and reaction durations of 5, 10, 15, and 20 min. After the mechanochemical treatment, the leachate and the solid residue ($FePO_4$) were separated by vacuum filtration. The elements in the leaching solution were analyzed by ICP–OES after acid digestion. The $FePO_4$ solid residue was rinsed and dried for material characterization. The Li metal in the leaching solution was recovered by carbon dioxide precipitation as a lithium carbonate (Li_2CO_3) product.

(III) Restoring the LFP crystals: using the recovered Li_2CO_3 and $FePO_4$ residues as raw materials, a regenerated $LiFePO_4$ cathode material was prepared using a high-temperature solid-phase method.[31,37] The Li_2CO_3 and $FePO_4$ solid residues were uniformly mixed according to the Li : Fe : P molar ratio of 1.05 : 1 : 1. Subsequently, glucose with a mass ratio of 12 wt% was added and mixed in the planetary ball-milling device for 1 h at a rotational speed of 200 rpm. The decomposed glucose at high temperatures can serve as a carbon source to coat the surface of LFP crystals, thus improving the cathode material's electrochemical properties. Moreover, the reduction atmosphere generated by glucose decomposition promotes the conversion of Fe^{3+} to Fe^{2+}. The final solid products were gradient calcined under a helium atmosphere at 700 °C for 10 h. The regenerated black powder LFP cathode material (called R-LFP) was subjected to sample characterization and electrochemical testing. The electrochemical test steps for the cathode materials, including spent LFP, regenerated LFP, and commercial LFP (C-LFP), are provided in the ESI (Text S1†).[68]

2.3. Analytical methods

The elemental contents in the cathode electrode and spent LFP cathode materials were analyzed by ICP–OES after acid digestion (180 °C, HCl : HNO_3 1 : 1 v/v). The digestion procedure for the solution can be referred to in our previous study.[69] The elemental contents of the LFP cathode material are shown in Table S2.† The metal recovery was calculated using eqn (1):

$$m_0 = m_1/m_2 \times 100\% \tag{1}$$

where m_0 is the element leaching percentage (wt%), m_1 is the actual mass (g) of the elements in the filtrate after H_2O_2 leaching, and m_2 is the original mass (g) of the elements in the cathode electrode or LFP cathode material estimated by its complete acid digestion.

The mineralogical composition of the solid material was analyzed by X-ray diffraction analysis (XRD; Rigaku SmartLab, Japan). X-ray photoelectron spectroscopy (XPS, ESCALAB 250Xi spectrometer, U.S.A.) was executed to reveal the elemental surface chemistry on the material surface. A Fourier-transform infrared spectrometer (FT–IR, PerkinElmer, USA, range:

4000–400 cm^{-1}, total 25 scans) was used to confirm the change in the surface functional group on the electrode surface. High-resolution transmission electron microscopy–mapping measurements were carried out with 200 keV electrons using a Titan G2 60–300 (HR–TEM–Mapping; FEI, U.S.A.) device with an image corrector. The distribution of elements in LFP crystals was tested using a Time-of-Flight Secondary Ion Mass Spectrometry (TOF-SIMS) 5 instrument (ION-TOF GmbH, Münster, Germany).

2.4. Life cycle assessment

A life cycle assessment (LCA) was conducted to assess the environmental impact of the designed route. An industrialized pyrometallurgical and hydrometallurgical combined process was established as a control. The effects of substance consumption and energy demand were quantified using SimaPro 8.5 software (PRé Sustainability, Netherlands).[70] The evaluation procedure adopted was TRACI 2.1 V1.06/US 2008. Ten indicators, such as global warming potential (GWP, kg CO_2 eq.), smog (PS, kg O_3 eq.), ozone depletion (OD, kg CFC-11 eq.), acidification (AC, mol SO_2 eq.), eutrophication (EU, kg N eq.), carcinogenic (HHC, CTUh), non-carcinogenic (HHNC, CTUh), respiratory effects (RE, kg PM2.5 eq.), ecotoxicity (EC, CTUe), and fossil fuel depletion (FF, MJ surplus), were selected to comprehensively describe the impact of the process life cycle. Ecoinvent 3 and the U.S. Life Cycle Inventory (USLCI) databases were used as the major inventories to emphasize gate-to-gate environmental impacts.[71] Life cycle boundaries for the established process are shown in Fig. S1 and S2.† The calculation details are provided in Text S2 and Tables S3–S6 in the ESI.†

3. Results and discussion

3.1. Hydro-oxygen separation of the cathode electrode

The efficiency of cathode electrode separation in a hydro-oxygen environment was investigated. The contents of Li, Fe, P, and Al in the solution generally increased with increasing H_2O_2 concentration and time (Fig. 2a and b). Li had the highest content among the leached elements during the separ-

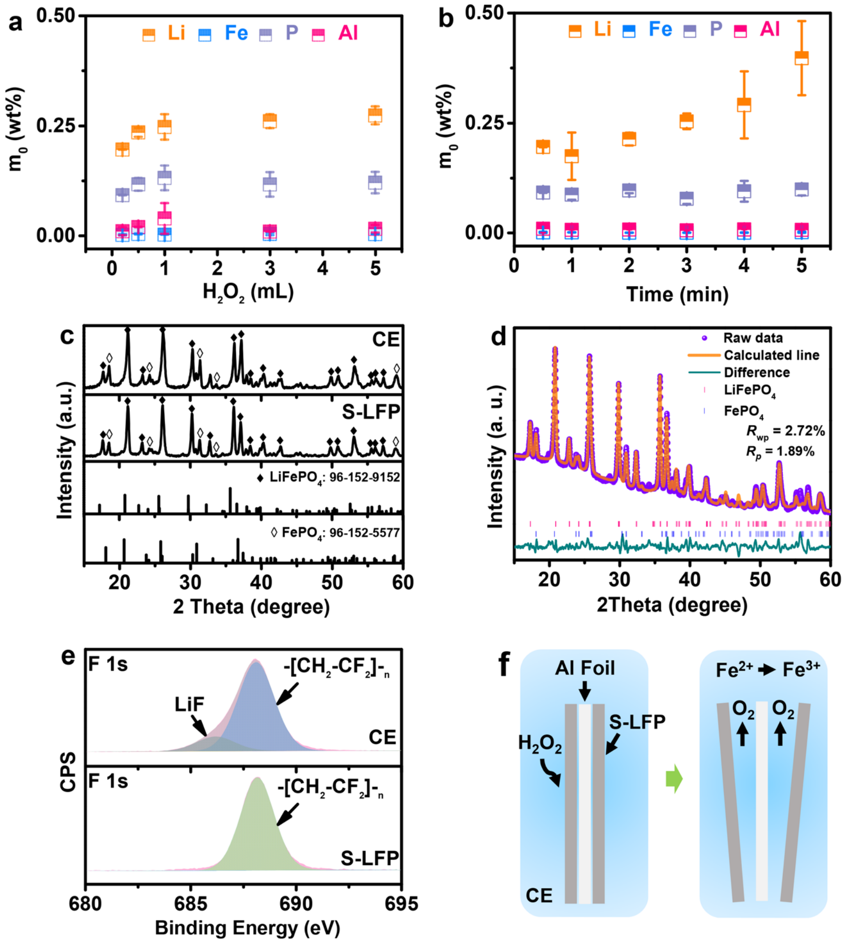

Fig. 2 Effects of (a) H_2O_2 addition and (b) reaction time on the leaching percentages of elements during the hydro-oxygen separation (conditions: a solution volume of 50.0 mL; (a) a time of 0.25 min and a cathode electrode : H_2O_2 ratio of 2.5 : 1 g mL^{-1} and (b) a cathode electrode : H_2O_2 ratio of 2.5 : 1 g mL^{-1}); (c) XRD patterns of the original cathode electrode and spent LFP, (d) Rietveld refinement of the spent LFP, (e) F 1s high-resolution energy spectra of the cathode electrode and spent LFP; and (f) the separation mechanism of spent LFP and Al foil (CE represents the cathode electrode).

ation stage. Nevertheless, the leaching percentage of Li was only 0.2–0.4 wt%, demonstrating that the hydro-oxygen environment can avoid massive loss of Li from LFP crystals while separating spent LFP cathode materials and the Al foil in a very short time (0.25 minutes). According to the pH changes (Fig. S3†), the acidic hydro-oxygen environment may be the main cause of slight Li loss. The leaching of P may result from the lithium phosphate formed during the operation of LFP batteries.[60] In contrast, the leaching of Fe and Al was negligible. As the cathode electrode : H_2O_2 ratio increased, the loss of elements from the spent LFP cathode materials decreased (Fig. S4†). When the cathode electrode : H_2O_2 ratio was 30 : 1 g mL^{-1}, the cathode electrode could still be completely separated, indicating the hydro-oxygen environment's high specific capacity for exfoliating spent LFP cathode materials. Therefore, the optimal hydro-oxygen separation conditions were 0.25 minutes at a cathode electrode : H_2O_2 ratio of 30 : 1 g mL^{-1}. Additionally, H_2O_2 is relatively stable at room temperature when used as a stripping agent, so conducting experiments at room temperature can help avoid any loss of H_2O_2.

The LFP crystals before and after hydro-oxygen separation were consistent with the standard Joint Committee for Powder Diffraction File (JCPDF) card (#96-152-9152), confirming that the spent LFP crystals could be maintained in a hydro-oxygen environment (Fig. 2c). The XRD patterns of spent LFP were analyzed using the Rietveld method with the Gauss function and pseudo-Voigt equation (Fig. 2d). The results showed that the fitting parameter full spectrum factor (R_p) and weighted full spectrum factor (R_{wp}) of differential peaks were 1.89% and 2.72%, respectively. Nearly 11.5% of the $FePO_4$ phase was observed in the spent LFP due to Li vacancies. The loss of Li was attributed to the migration failure during the service life of the LFP battery. XPS high-resolution energy spectra of Li 1s (Fig. S5a†), Fe 2p (Fig. S5b†), and P 2p (Fig. S5c†) indicated that the elemental environment on the surface of the cathode materials remained unchanged, confirming that the hydro-oxygen environment could effectively protect spent LFP crystals from deconstruction. Furthermore, the XRD patterns of the peeled Al foil were consistent with the standard JCPDF card of metallic Al (No# 00-001-1180) (Fig. S6†). According to actual observation, the surfaces of the Al foil and spent LFP remained smooth (Fig. S7†). Based on EDAX (Fig. S8†) and additional XPS analyses, the F content detected on the surface of the Al foil was found to be only 0.66 wt% and 1.44 wt%, respectively. This low level of F content on the surface of the aluminum foil implies that the foil can be directly recycled without any need for secondary processing. Before the hydro-oxygen reaction, the binding energies of F 1s corresponded to PVDF and lithium fluoride (LiF) (Fig. 2e). After the hydro-oxygen reaction, only the characteristic peaks of PVDF were observed. The leaching percentage of F was lower than 1.5 wt% (Fig. S9†), while organic F still existed on the surface of the spent LFP in the form of PVDF (Fig. S10†). Therefore, the lost Li species may be the LiF species in the solid electrolyte interphase film formed during battery use. After concentration, a small amount of LiF (0.41 wt%) in solution can be recovered as the Li_2CO_3 product by using the precipitation method with sodium carbonate. Overall, the separation of the cathode electrode in the hydro-oxygen environment can be attributed to the Fenton reaction of Fe^{2+} in the spent LFP crystal with H_2O_2 (Fig. 2f).[72,73] As the binding force of PVDF between the spent LFP and the Al foil was relatively weak, rapid and non-destructive separation could be achieved from the pressure gradient introduced by the released oxygen bubbles.[74]

3.2. Hydro-oxygen extraction of lithium

When the redox potential of the liquid-phase system increased, Li embedded in LFP crystals was released into the hydro-oxygen solution, and a phase transition of the LFP crystal to $FePO_4$ was induced (Fig. 3a).[75,76] In a hydro-oxygen environment containing LFP/H_2O_2, Li was transformed into a soluble state (LiOOH or lithium hydroperoxide) and separated from the $FePO_4$ framework due to the increase in the chemical potential and decrease in pH. With an increase in H_2O_2 concentration, the bending vibration of tetrahedral PO_4 located at 532 and 576 cm^{-1} and the stretching vibration of octahedral FeO_6 located at 647 and 686 cm^{-1} were gradually observed in the range of 500–800 cm^{-1}, indicating the de-intercalation of Li (Fig. 3b). The characteristic band of olivine $FePO_4$ at 1236 cm^{-1} was observed in the solid residues, which could not be identified in the spent LFP. Furthermore, the symmetric stretching mode of PO_4^{3-} in LFP gradually shifted from the

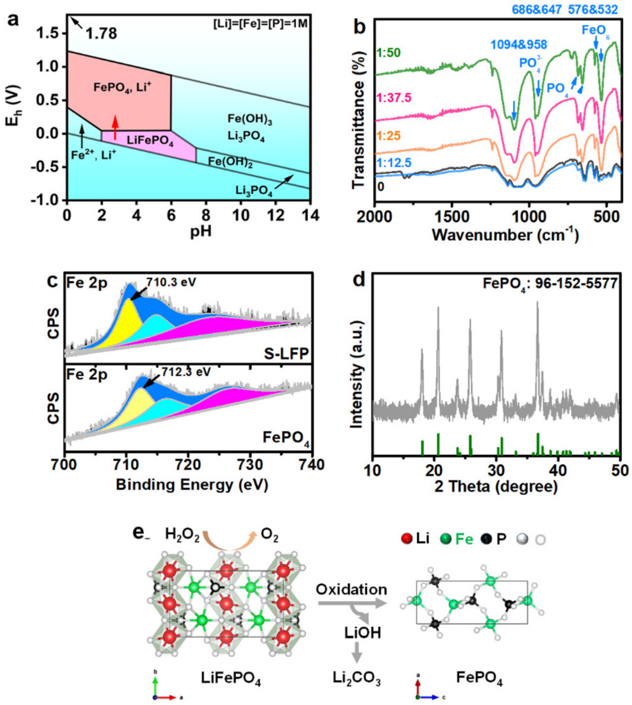

Fig. 3 (a) E_h–pH diagram for the Li–Fe–P–H_2O system at 298.15 K (data were obtained from the HSC chemistry 6.0 software), (b) FT-IR spectra of the residues after Li extraction with different H_2O_2 amounts, (c) Fe 2p spectra before (spent LFP) and after ($FePO_4$) Li extraction, (d) XRD patterns of the $FePO_4$ solid residue, and (e) the oxidative extraction mechanism of Li.

energy band of 973 cm^{-1} to 959 cm^{-1} in $FePO_4$, confirming the formation of $FePO_4$.[31] After hydro-oxygen extraction, the binding energy of Fe $2p_{3/2}$ shifted from 710.3 eV ($LiFePO_4$ species) to 712.3 eV ($FePO_4$ species) (Fig. 3c).[77] Additionally, the XRD patterns demonstrated the phase transition of LFP crystals to $FePO_4$, confirming the successful extraction of Li (Fig. 3d). The leaching concentration of Li in the hydro-oxygen environment reached 23.7 mg L^{-1}, along with P of 5.7 mg L^{-1}, Fe of 0.8 mg L^{-1}, and Al of 0.1 mg L^{-1}, which are considered low levels and insignificant (Fig. S11†).

In our proposed method, the only reagent used in the integrated HOR route was H_2O_2, thus avoiding interference caused by the introduction of impurities of exogenous cations and anions. Li in the liquid phase was concentrated and selectively recovered by chemical precipitation. The XRD patterns of the obtained Li_2CO_3 products (Fig. S12†) were consistent with the standard JCPDF card (#01-087-0729), which appeared to exhibit an irregular granular structure. The oxidative extraction mechanism of Li is elucidated in Fig. 3e. In the presence of H_2O_2, Fe^{2+} in spent LFP could be oxidized to Fe^{3+}, and the LFP crystals released Li^+. The leached Li^+ was combined with hydroxide and converted into soluble LiOH. The mechanochemical extraction parameters of Li are shown in Fig. S13.† The sealed mechanochemical oxidation environment not only improved the extraction efficiency of Li but also directly generated the leaching of Li from spent LFP, thereby reducing the emission of dust in practical application.[78] The optimal parameters were a solid/liquid ratio of 1 : 37.5 g mL^{-1}, 10 min, and 1000 rpm, under which the initial leaching efficiency of Li could reach up to 83.0 wt%.

3.3. Regeneration of $LiFePO_4$ crystals

The process of pre-lithiation was characterized using TOF-SIMS. The scale of element concentration has been highlighted in brown font. A small amount of Li remained in the initial $FePO_4$ leaching framework (Fig. 4a), which was attributed to the incomplete deintercalation of Li during the mechanochemical oxidative extraction. After Li intercalation and high-temperature annealing, the concentration of Li in the regenerated LFP was significantly enhanced, and its crystal structure could be recovered (Fig. 4b). The characteristic diffraction peaks of the reshaped crystals were composed of a single olivine-structured $LiFePO_4$ phase (JCSPD no. 96-400-1847) (Fig. 4c). According to the Rietveld refinement (Fig. 4c), the R_p and R_{wp} were 1.17%, and 1.86%, respectively, and the error factor (χ^2) was 8.211, indicating that the lattice structure of the reshaped regenerated LFP was very close to the theoretical crystalline state. The Rietveld refinement results further demonstrated that the regenerated LFP crystals were well crystallized in the orthorhombic structure *Pnma* (62). The lattice parameters of *a*, *b*, and *c* were 6.010 Å, 10.334 Å, and 4.694 Å, respectively, with a corresponding volume of 291.556 $Å^3$, confirming the reshaping of the regenerated LFP crystal. The TEM-SAED results of the $FePO_4$ framework are shown in Fig. S14.† The regenerated LFP cathode materials characterized by an irregular round particle can be observed in Fig. 4d (I). As shown, the surface of regenerated LFP was covered by a layer of amorphous carbon (Fig. 4d (II)). The LFP crystals had a clear lattice spacing with a distance of 0.230 nm, fitting the spacing of the (012) planes by $LiFePO_4$ (JCPDS card no. 00-040-1499) (Fig. 4d (III and IV)). The fast Fourier transform results (Fig. 4d (V)) show the nano-single crystal characteristic of the regenerated LFP with the (012), (112), and (101) crystal planes. The above results demonstrate that Li could re-enter the olivine framework structure of $FePO_4$, and the regenerated LFP crystals could be successfully restored after pre-lithiation and annealing in the proposed approach.

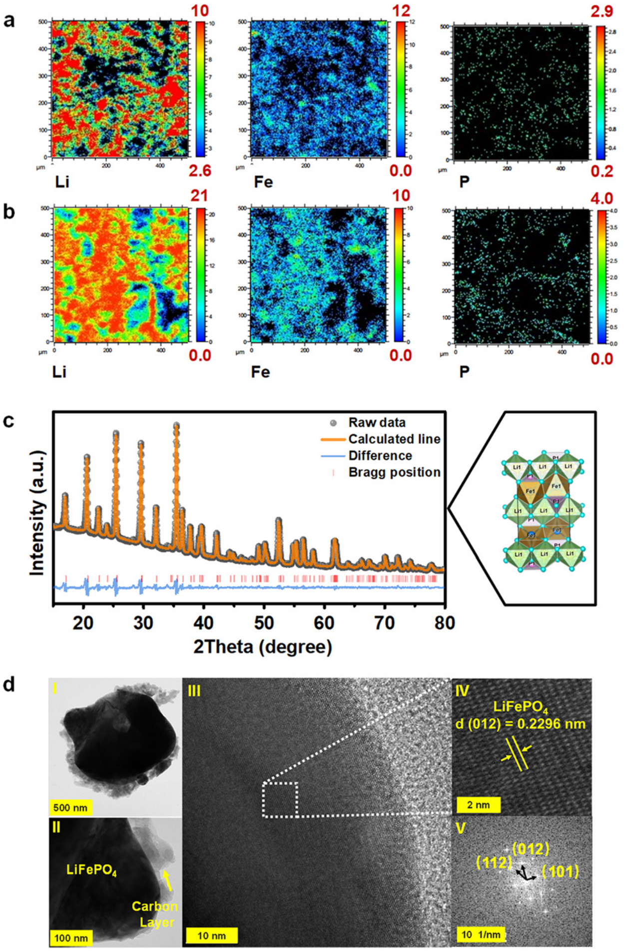

Fig. 4 TOF-SIMS mapping of (a) the initial $FePO_4$ leaching residue and (b) regenerated LFP; (c) Rietveld refinement of the regenerated LFP; and (d) TEM/HRTEM images (I: TEM at 500 nm scale, II: TEM at 100 nm scale, III: HRTEM at 10 nm scale, IV: HRTEM at 2 nm scale, and V: fast Fourier transform results of the regenerated LFP and the width of the yellow box is the corresponding scale).

3.4. Electrochemical performance

The coin cells were assembled to verify the performance of the prepared regenerated LFP for practical applications and to compare the regenerated LFP with commercial LFP and spent LFP. The charge/discharge curves of Li||LFP coin cells at 0.1C are shown in Fig. 5a, which display that the polarization of the regenerated LFP coin cells was lower than those of the commer-

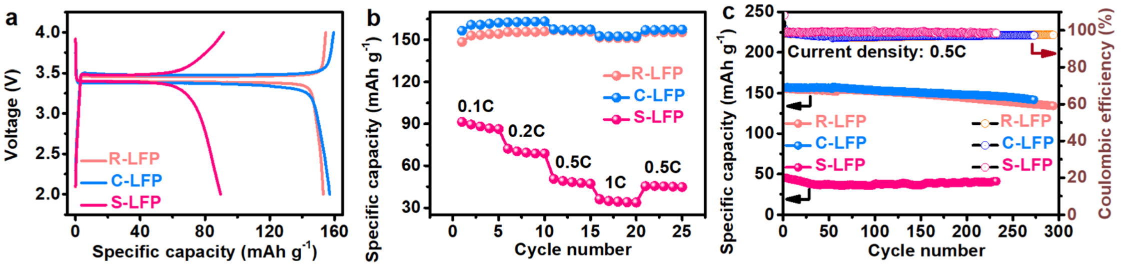

Fig. 5 (a) Charge/discharge curves of Li||LFP full batteries in the 1st cycle, (b) rate capability of Li||LFP full batteries, and (c) cycling performance and coulombic efficiency of Li||LFP full batteries.

cial LFP and spent LFP. According to Ohm's law, the greater the internal resistance, the greater the polarization, so the internal resistance can be judged by polarization. The minimum polarization of regenerated LFP indicates that its internal resistance was the smallest. This implies that the regenerated LFP coin cells had less internal resistance, which was conducive to the long-term stable cycling of the regenerated batteries. Although the initial discharge capacity of commercial LFP was higher, its first-cycle coulombic efficiency (98.1%) was slightly lower than that of regenerated LFP (99.1%). Fig. 5b shows the rate performance tests under different current densities. Although the regenerated LFP had a lower specific capacity at the initial two current densities than the commercial LFP, the regenerated LFP showed a specific capacity (~151.2 mA h g^{-1}) nearly comparable to that of the commercial LFP (~152.5 mA h g^{-1}) at a high rate (1C). While the spent LFP displayed the lowest specific capacity at each rate, especially when the rate returned 0.1C, the specific capacity significantly decreased compared with the initial 0.1C cycle. Based on the above analysis, the regenerated LFP illustrated a high first-cycle coulombic efficiency and a long-cycle performance similar to the commercial LFP. Therefore, the regenerated LFP is believed to be a promising $LiFePO_4$ cathode material. The initial specific capacity of regenerated LFP was 155.6 mA h g^{-1}, which reached the level of commercial LFP. Meanwhile, the capacity retention ratio of regenerated LFP was maintained at 87.9% (Fig. 5c) after 270 cycles under 0.5C, which was very close to that of commercial LFP (90.5%). Together with a stable coulombic efficiency, the regenerated LFP showed a high degree of cycling stability. It is expected that the coin cell with the spent LFP exhibited a low specific capacity below 50 mA h g^{-1}.

3.5. Life cycle assessment

The environmental impacts of HOR were assessed using LCA. Pyrometallurgy and hydrometallurgy (Pyro & Hydro) were built as a control process to highlight the environmental contribution of the proposed HOR approach. Fig. 6a shows the relative environmental benefits of HOR and Pyro & Hydro processes. The 10 indicators of the HOR were all greater than zero, indicating that the HOR process can demonstrate a positive impact on the global environment. Compared to Pyro & Hydro processes, HOR showed better environmental benefits for the following indicators: GWP, PS, OD, AC, EU, HHNC, RE, and EC. Pyro & Hydro processes at GWP and PS clearly exhibited a negative impact on the ecosystem. The adverse factors of HOR and Pyro & Hydro processes at GWP and PS can be attributed to the input of chemicals and power. However, the harvest of Al foil, plastic, and $LiFePO_4$ cathode materials (Fig. S15,†

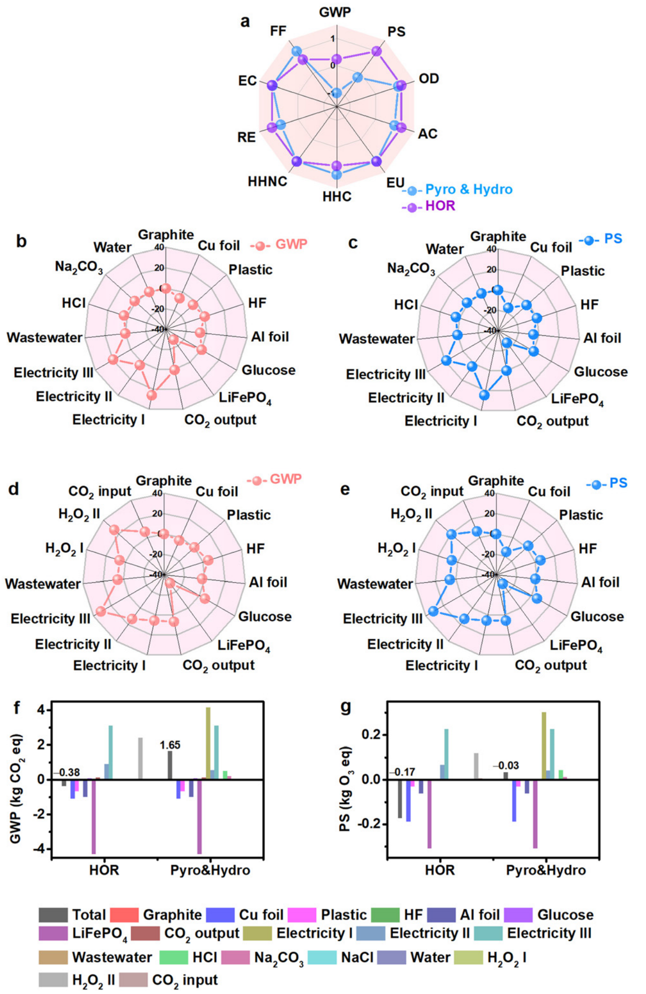

Fig. 6 (a) Relative environmental benefits of HOR and Pyro & Hydro; percentage contribution analysis of different parameters: (b) GWP (Pyro & Hydro), (c) PS (Pyro & Hydro), (d) GWP (HOR), and (e) PS (HOR); numerical contribution analysis of different parameters: (f) GWP and (g) PS (remarks: in (b)–(g), negative values indicate the reduced environmental impacts due to recycling and positive values indicate the environmental impacts due to input; details are provided in Tables S3–S6†).

Fig. 6b–e) from the recycling system can offset the production and manufacturing of raw materials, thus reducing the indicator values of GWP and PS. Excessive electricity I becomes the main negative factor for GWP and PS in the Pyro & Hydro processes (Fig. 6b and c). The high-efficiency separation of the cathode electrode in the hydro-oxygen environment of the HOR route significantly reduced the carbon footprint and smog (Fig. 6d and e). Notably, the synthesized LFP contributed to the largest reduction of carbon emission and smog, confirming the low-carbon feasibility and benefits of LFP regeneration (Fig. 6f and g). Based on the unit of recycling 1.0 kg of the spent LFP battery, the CO_2 emissions of HOR and Pyro & Hydro processes were −0.38 kg CO_2 eq. and 1.65 kg CO_2 eq., respectively (Fig. 6f). The PS was −0.17 kg O_3 eq. and 0.03 kg O_3 eq., respectively (Fig. 6g). The estimated recycling amount of discarded LFP batteries in China in 2022 is 83 000 tons (Shanghai Metals Market). Therefore, the potential for CO_2 emission reduction by using the HOR process can be 31 500 tons, which is likely to further increase in the coming years. In addition, the theoretical gains for HOR and Pyro & Hydro processes were 23.55 and 21.87 USD per kg, respectively (Table S7†). Based on the above analysis, the HOR process can be identified as a potentially low-carbon technology for recycling and restoring the spent LFP batteries in a new era of EVs.

4. Conclusions

High carbon emissions, use of corrosive reagents, and low profit margins are currently the main obstacles to the green recycling of spent LFP batteries. The present study was designed to develop a facile, cost-effective, low-carbon, and scalable HOR route to recover and regenerate spent LFP batteries. Hydro-oxygen separation provided rapid and non-destructive separation of cathode materials and Al foil in 0.25 minutes, avoiding environmental concerns regarding dust/pollutant emissions and Li loss. Subsequent hydro-oxygen oxidative extraction of residual lithium from peeled $LiFePO_4$ cathode materials enabled efficient and rapid pre-lithiation of spent LFP cathode materials (83.0 wt% in 10 minutes) without introducing impurities. The performance of the regenerated LFP battery presented an initial specific capacity of 155.6 mA h g^{-1} at 1C and was able to restore a capacity retention ratio of 87.9% after 270 cycles under 0.5C, which was comparable to those of new power LIBs. Life cycle assessment confirmed that our proposed HOR route can significantly reduce the carbon footprint (−0.38 kg CO_2 eq.) when recycling each kg of spent LFP batteries, representing a potentially low-carbon and green approach towards global decarbonization.

Author contributions

Kang Liu: conceptualization, data curation, and writing – original draft preparation. Junxiong Wang: methodology, formal analysis, and data curation. Mengmeng Wang: methodology, investigation, and reviewing. Qiaozhi Zhang: methodology and reviewing. Yang Cao: methodology and reviewing. Longbin Huang: reviewing. Marjorie Valix: reviewing. Daniel C. W. Tsang: methodology, supervision, funding acquisition, and reviewing.

Conflicts of interest

The authors declare no competing financial interest.

Acknowledgements

This research was supported by the Hong Kong Research Grants Council (PolyU 15231522) and the National Natural Science Foundation of China (51908318).

References

1 X. Sun, H. Hao, F. Zhao and Z. Liu, *Environ. Sci. Technol.*, 2018, **53**, 743–751.

2 O. Y. Edelenbosch, A. F. Hof, B. Nykvist, B. Girod and D. P. Van Vuuren, *Clim. Change*, 2018, **151**, 95–108.

3 Ö. Andersson and P. Börjesson, *Appl. Energy*, 2021, **289**, 116621.

4 A. Khajuria, V. A. Atienza, S. Chavanich, W. Henning, I. Islam, U. Kral, M. Liu, X. Liu, I. K. Murthy, T. D. T. Oyedotun, P. Verma, G. Xu, X. Zeng and J. Li, *Circ. Econ.*, 2022, **1**, 100001.

5 M. Wang, K. Liu, S. Dutta, D. S. Alessi, J. Rinklebe, Y. S. Ok and D. C. Tsang, *Renewable Sustainable Energy Rev.*, 2022, **163**, 112515.

6 C. IEA, URL: https://www.iea.org/reports/global-ev-outlook-2020, 2020.

7 M. U. Ali, A. Zafar, S. H. Nengroo, S. Hussain, M. Junaid Alvi and H.-J. Kim, *Energies*, 2019, **12**, 446.

8 M. Armand, P. Axmann, D. Bresser, M. Copley, K. Edström, C. Ekberg, D. Guyomard, B. Lestriez, P. Novák and M. Petranikova, *J. Power Sources*, 2020, **479**, 228708.

9 L. Saw, K. Somasundaram, Y. Ye and A. Tay, *J. Power Sources*, 2014, **249**, 231–238.

10 X.-G. Yang, T. Liu and C.-Y. Wang, *Nat. Energy*, 2021, **6**, 176–185.

11 X. Zhang, H. Peng, H. Wang and M. Ouyang, *IEEE Trans. Veh. Technol.*, 2017, **67**, 956–965.

12 S. Chen, M. Chen, J. Shu and Y. Deng, *Circ. Econ.*, 2022, **1**, 100013.

13 E. A. Olivetti, G. Ceder, G. G. Gaustad and X. Fu, *Joule*, 2017, **1**, 229–243.

14 T. Watari, K. Nansai and K. Nakajima, *Resour., Conserv. Recycl.*, 2020, **155**, 104669.

15 X. Fu, D. N. Beatty, G. G. Gaustad, G. Ceder, R. Roth, R. E. Kirchain, M. Bustamante, C. Babbitt and E. A. Olivetti, *Environ. Sci. Technol.*, 2020, **54**, 2985–2993.

16 Z. Yang, H. Huang and F. Lin, *Adv. Energy Mater.*, 2022, 2200383.

17 C. P. Makwarimba, M. Tang, Y. Peng, S. Lu, L. Zheng, Z. Zhao and A.-G. Zhen, *iScience*, 2022, 104321.

18 Y. Miao, L. Liu, Y. Zhang, Q. Tan and J. Li, *J. Hazard. Mater.*, 2022, **425**, 127900.

19 G. Zubi, R. Dufo-López, M. Carvalho and G. Pasaoglu, *Renewable Sustainable Energy Rev.*, 2018, **89**, 292–308.

20 S. Natarajan and V. Aravindan, *Adv. Energy Mater.*, 2018, **8**, 1802303.

21 W. Liu, H. Liu, W. Liu and Z. Cui, *Renewable Sustainable Energy Rev.*, 2021, **139**, 110596.

22 X. Lai, Y. Huang, C. Deng, H. Gu, X. Han, Y. Zheng and M. Ouyang, *Renewable Sustainable Energy Rev.*, 2021, **146**, 111162.

23 M. Fan, X. Chang, Q. Meng, L.-J. Wan and Y.-G. Guo, *SusMat*, 2021, **1**, 241–254.

24 C. Liu, J. Lin, H. Cao, Y. Zhang and Z. Sun, *J. Cleaner Prod.*, 2019, **228**, 801–813.

25 M. Kaya, *Circ. Econ.*, 2022, **1**, 100015.

26 F. Forte, M. Pietrantonio, S. Pucciarmati, M. Puzone and D. Fontana, *Crit. Rev. Environ. Sci. Technol.*, 2021, **51**, 2232–2259.

27 Y. Dai, Z. Xu, D. Hua, H. Gu and N. Wang, *J. Hazard. Mater.*, 2020, **396**, 122707.

28 H. Mahandra and A. Ghahreman, *Resour., Conserv. Recycl.*, 2021, **175**, 105883.

29 K. He, Z.-Y. Zhang and F.-S. Zhang, *J. Hazard. Mater.*, 2020, **395**, 122614.

30 Y. Yang, X. Meng, H. Cao, X. Lin, C. Liu, Y. Sun, Y. Zhang and Z. Sun, *Green Chem.*, 2018, **20**, 3121–3133.

31 H. Jin, J. Zhang, D. Wang, Q. Jing, Y. Chen and C. Wang, *Green Chem.*, 2022, **24**, 152–162.

32 N. Singh and O. A. Ogunseitan, *Circ. Econ.*, 2022, **1**, 100011.

33 P. Yadav, C. J. Jie, S. Tan and M. Srinivasan, *J. Hazard. Mater.*, 2020, **399**, 123068.

34 W. Wang and Y. Wu, *Resour., Conserv. Recycl.*, 2017, **127**, 233–243.

35 B. Zhang, X. Qu, X. Chen, D. Liu, Z. Zhao, H. Xie, D. Wang and H. Yin, *J. Hazard. Mater.*, 2022, **424**, 127586.

36 J. Yu, X. Wang, M. Zhou and Q. Wang, *Energy Environ. Sci.*, 2019, **12**, 2672–2677.

37 X. Qiu, B. Zhang, Y. Xu, J. Hu, W. Deng, G. Zou, H. Hou, Y. Yang, W. Sun and Y. Hu, *Green Chem.*, 2022, **24**, 2506–2515.

38 X. Lai, Y. Huang, H. Gu, C. Deng, X. Han, X. Feng and Y. Zheng, *Energy Storage Mater.*, 2021, **40**, 96–123.

39 B. Gangaja, S. Nair and D. Santhanagopalan, *ACS Sustainable Chem. Eng.*, 2021, **9**, 4711–4721.

40 B. Chen, M. Liu, S. Cao, G. Chen, X. Guo and X. Wang, *Mater. Chem. Phys.*, 2022, **279**, 125750.

41 X. Tang, R. Wang, Y. Ren, J. Duan, J. Li and P. Li, *J. Mater. Sci.*, 2020, **55**, 13036–13048.

42 N. Paul, J. Wandt, S. Seidlmayer, S. Schebesta, M. J. Mühlbauer, O. Dolotko, H. A. Gasteiger and R. Gilles, *J. Power Sources*, 2017, **345**, 85–96.

43 M. Ouyang, Z. Chu, L. Lu, J. Li, X. Han, X. Feng and G. Liu, *J. Power Sources*, 2015, **286**, 309–320.

44 S. Xu, K.-H. Chen, N. P. Dasgupta, J. B. Siegel and A. G. Stefanopoulou, *J. Electrochem. Soc.*, 2019, **166**, A3456.

45 Z. Yang, Y. Dai, S. Wang and J. Yu, *J. Mater. Chem. A*, 2016, **4**, 18210–18222.

46 M. Arnaiz and J. Ajuria, *Batteries Supercaps*, 2021, **4**, 733–748.

47 L. Jin, C. Shen, Q. Wu, A. Shellikeri, J. Zheng, C. Zhang and J. P. Zheng, *Adv. Sci.*, 2021, **8**, 2005031.

48 P. Xu, Q. Dai, H. Gao, H. Liu, M. Zhang, M. Li, Y. Chen, K. An, Y. S. Meng and P. Liu, *Joule*, 2020, **4**, 2609–2626.

49 Q. Jing, J. Zhang, Y. Liu, W. Zhang, Y. Chen and C. Wang, *ACS Sustainable Chem. Eng.*, 2020, **8**, 17622–17628.

50 P. Liu, Y. Zhang, P. Dong, Y. Zhang, Q. Meng, S. Zhou, X. Yang, M. Zhang and X. Yang, *J. Alloys Compd.*, 2021, **860**, 157909.

51 W. Song, J. Liu, L. You, S. Wang, Q. Zhou, Y. Gao, R. Yin, W. Xu and Z. Guo, *J. Power Sources*, 2019, **419**, 192–202.

52 D. Peng, J. Zhang, J. Zou, G. Ji, L. Ye, D. Li, B. Zhang and X. Ou, *J. Cleaner Prod.*, 2021, **316**, 128098.

53 J. Li, Y. Wang, L. Wang, B. Liu and H. Zhou, *J. Mater. Sci.: Mater. Electron.*, 2019, **30**, 14580–14588.

54 W. Lv, Z. Wang, H. Cao, Y. Sun, Y. Zhang and Z. Sun, *ACS Sustainable Chem. Eng.*, 2018, **6**, 1504–1521.

55 G. Zhang, X. Yuan, Y. He, H. Wang, T. Zhang and W. Xie, *J. Hazard. Mater.*, 2021, **406**, 124332.

56 Y. He, X. Yuan, G. Zhang, H. Wang, T. Zhang, W. Xie and L. Li, *Sci. Total Environ.*, 2021, **766**, 142382.

57 H. Huang, C. Liu and Z. Sun, *J. Hazard. Mater.*, 2022, **435**, 128974.

58 X. Zeng, J. Li and N. Singh, *Crit. Rev. Environ. Sci. Technol.*, 2014, **44**, 1129–1165.

59 J. Ordoñez, E. J. Gago and A. Girard, *Renewable Sustainable Energy Rev.*, 2016, **60**, 195–205.

60 K. He, Z.-Y. Zhang and F.-S. Zhang, *J. Hazard. Mater.*, 2020, **386**, 121633.

61 M. Wang, Q. Tan, L. Liu and J. Li, *ACS Sustainable Chem. Eng.*, 2020, **8**, 7489–7496.

62 X. Zhong, W. Liu, J. Han, F. Jiao, W. Qin, T. Liu and C. Zhao, *Waste Manage.*, 2019, **89**, 83–93.

63 X. Zhang, L. Li, E. Fan, Q. Xue, Y. Bian, F. Wu and R. Chen, *Chem. Soc. Rev.*, 2018, **47**, 7239–7302.

64 Y. Li, W. Lv, H. Huang, W. Yan, X. Li, P. Ning, H. Cao and Z. Sun, *Green Chem.*, 2021, **23**, 6139–6171.

65 Y. Zhang, Y. Wang, H. Zhang, Y. Li, Z. Zhang and W. Zhang, *Resour., Conserv. Recycl.*, 2020, **156**, 104688.

66 X. Song, T. Hu, C. Liang, H. Long, L. Zhou, W. Song, L. You, Z. Wu and J. Liu, *RSC Adv.*, 2017, **7**, 4783–4790.

67 M. Wang, K. Liu, J. Yu, C.-C. Zhang, Z. Zhang and Q. Tan, *Circ. Econ.*, 2022, 100012.

68 J. Wang, Z. Liang, Y. Zhao, J. Sheng, J. Ma, K. Jia, B. Li, G. Zhou and H.-M. Cheng, *Energy Storage Mater.*, 2022, **45**, 768–776.

69 K. Liu, M. Wang, Q. Zhang, Z. Xu, C. Labianca, M. Komárek, B. Gao and D. C. Tsang, *J. Hazard. Mater.*, 2023, **445**, 130502.

70 F. Wu, Z. Zhou and A. L. Hicks, *Environ. Sci. Technol.*, 2019, **53**, 4078–4087.

71 F. Wu, Z. Zhou, S. Temizel-Sekeryan, R. Ghamkhar and A. L. Hicks, *J. Cleaner Prod.*, 2020, **270**, 122465.

72 Y. He, T. Zhang, F. Wang, G. Zhang, W. Zhang and J. Wang, *J. Cleaner Prod.*, 2017, **143**, 319–325.

73 L. Wu, F.-S. Zhang, X.-H. Yue and Z.-Y. Zhang, *J. Cleaner Prod.*, 2022, 133749.

74 X. Zhong, J. Han, L. Chen, W. Liu, F. Jiao, H. Zhu and W. Qin, *Appl. Surf. Sci.*, 2021, **553**, 149564.

75 J. Zhang, J. Hu, Y. Liu, Q. Jing, C. Yang, Y. Chen and C. Wang, *ACS Sustainable Chem. Eng.*, 2019, **7**, 5626–5631.

76 Q. Jing, J. Zhang, Y. Liu, C. Yang, B. Ma, Y. Chen and C. Wang, *J. Phys. Chem. C*, 2019, **123**, 14207–14215.

77 Z. Wu, J. Yang, W. Shao, M. Cheng, X. Luo, M. Zhou, S. Li, T. Ma, C. Cheng and C. Zhao, *Adv. Fiber Mater.*, 2022, **4**, 774–785.

78 M. Wang, K. Liu, J. Yu, C.-C. Zhang, Z. Zhang and Q. Tan, *Circ. Econ.*, 2022, **1**, 100012.